INTERNATIONAL JOURNAL FOR NUMERICAL METHODS IN FLUIDS
Int. J. Numer. Meth. Fluids 2005; **47**:139–159
Published online 5 November 2004 in Wiley InterScience (www.interscience.wiley.com). DOI: 10.1002/fld.801

A stabilized SPH method for inviscid shallow water flows‡

Riadh Ata§ and Azzeddine Soulaïmani*,†

Département de Génie Mécanique, École de technologie supérieure; 1100 Notre-Dame Ouest, Montréal, Qué., Canada H3C 1K3

SUMMARY

In this paper, the smoothed particle hydrodynamics (SPH) method is applied to the solution of shallow water equations. A brief review of the method in its standard form is first described then a variational formulation using SPH interpolation is discussed. A new technique based on the Riemann solver is introduced to improve the stability of the method. This technique leads to better results. The treatment of solid boundary conditions is discussed but remains an open problem for general geometries. The dam-break problem with a flat bed is used as a benchmark test. Copyright © 2004 John Wiley & Sons, Ltd.

KEY WORDS: SPH; meshless methods; free surface; shallow water; Riemann solver

1. INTRODUCTION

Free surface flows are often numerically solved using Eulerian approaches such as the finite volume or finite element methods. However, some difficulties related mainly to accuracy are faced in the presence of moving boundaries, such as the wetting–drying phenomena particularly important in flood simulations. In this paper, a purely Lagrangian and meshless approach, the smoothed particle hydrodynamics method (SPH), is investigated to explore its ability to solve shallow-water equations (SWE) in one and two space dimensions. SPH, the first and simplest of the meshless methods, is easy to implement. A new technique based on the use of Riemann solver is introduced to improve the stability of the method.

The SPH method was first introduced by Lucy [1] and Gingold and Monaghan [2] to simulate astrophysical problems. By the end of the 1980s and in the early 1990s, the SPH method became widely used with some other meshless methods especially in the simulation of high speed impacts and metal forming processes, see for instance the following references [3–7].

*Correspondence to: Azzeddine Soulaïmani, Département de Génie Mécanique, École de technologie supérieure; 1100 Notre-Dame Ouest, Montréal, Qué, Canada H3C 1K3.
†E-mail: azzeddine.soulaimani@etsmtl.ca
‡This research was funded by Hydro-Québec and the National Sciences and Engineering Research Council of Canada (NSERC).
§E-mail: riadh.ata@etsmtl.ca

 Received 17 October 2003

For more details on the SPH method and its applications, we refer to [8]. A thorough review of other classes of meshless methods can be found in Reference [9]. Inutsuka introduced a Riemann solver in the SPH formulation to evaluate the force acting on each particle [10]. Cha *et al.* [11] gave a new formulation of SPH (called GPH, Godunov-type particle hydrodynamics). GPH has almost the same philosophy as SPH but uses a Riemann solver to obtain the hydrodynamic acceleration and the rate of change of the internal energy. SPH is a truly meshless method based on the transformation of differential equations into integral ones which are then discretized using a distribution of moving particles. It has given relatively good results in the applications cited above. However, in its standard form, a problem remains with stability and serious difficulties are faced in the treatment of the solid boundary conditions [9], especially with irregular boundaries. These two issues will be discussed in this paper.

The next section briefly reviews the standard SPH method and shows its application to inviscid shallow water flows over flat beds. Section 3 describes the development of a stablized variational formulation which employs the SPH approximation. In Section 4, we discuss the boundary conditions issue and several numerical aspects. The last section presents computational results for one- and two-dimensional dam break problems, and draws conclusions.

2. PROBLEM SETTING

Several works were devoted to free surface flows applying the SPH method, for example, References [12–14]. The mathematical model was based on the gas dynamic equations using an isentropic state law

$$p = k\left[\left(\frac{\rho}{\rho_0}\right)^{\gamma} - 1\right]$$

where p is the pressure, ρ is the density, γ is a parameter chosen as $\gamma = 7$. The bulk modulus employed is derived so that the Mach number of the flow is small (typically 0.1–0.01). Wang *et al.* [15] used the standard SPH method for one-dimensional SWE. Unfortunately, the results reported are 'unreproducible'. The numerical solution matches exact one perfectly, even in the presence of shocks. It is well documented [7, 8, 11, 16, 17], that some oscillations are present near the shocks even using the Monaghan shock-capturing viscosity.

In the following, we seek the numerical solution of the inviscid SWE in the non-conservative form neglecting the bed slope and friction terms (see Reference [18] for the application of SWE with source terms using Godunov methods)

$$\frac{\mathrm{D}h}{\mathrm{D}t} + h\nabla\cdot\mathbf{u} = 0 \tag{1}$$

$$\frac{\mathrm{D}\mathbf{u}}{\mathrm{D}t} + g\nabla h = 0 \tag{2}$$

where h, $\mathbf{u}$ and g are, respectively, water height, depth-averaged velocity, and gravity. $\mathrm{D}/\mathrm{D}t$ refers to the total derivative.

2.1. Review of the SPH method

The SPH method is based on the following identity: any generic function $f(\mathbf{x})$ can be obtained using the Dirac delta distribution centred at $\mathbf{x}$ as

$$f(\mathbf{x}) = \int_\Omega f(\mathbf{s})\delta(\mathbf{x}-\mathbf{s})\,\mathrm{d}s \tag{3}$$

where Ω is the domain of definition of f. In practice, the Dirac distribution is approximated by a more regular function W called the 'kernel' which has to satisfy several mathematical constraints [19, 20],

$$f(\mathbf{x}) \simeq \int_\Omega f(\mathbf{s})W(\mathbf{x}-\mathbf{s})\,\mathrm{d}\mathbf{s} \tag{4}$$

The kernel depends on the variable $\mathbf{x}-\mathbf{s}$ and on a second variable l, called the smoothing length. Gauss and spline kernels are commonly used in practice, have the important property of being symmetric kernels (or even kernels, i.e. $W(\mathbf{x}-\mathbf{s}) = W(\mathbf{s}-\mathbf{x})$) with antisymmetric gradient (i.e. $\partial W(\mathbf{x}-\mathbf{s})/\partial\mathbf{x} = -\partial W(\mathbf{x}-\mathbf{s})/\partial\mathbf{s}$). Among the constraints on the kernel are: (normalized kernel) $\int_\Omega W(\mathbf{x}-\mathbf{s})\,\mathrm{d}\mathbf{s} = 1$ and (kernel with compact support) $W(\mathbf{x}-\mathbf{s}) = 0$ for $\|\mathbf{x}-\mathbf{s}\| \geqslant \kappa l$, with κ a positive integer. Using an integration by parts and the compact support property of the kernel, the derivative of f with respect to the variable x^m is given by

$$\frac{\partial f(\mathbf{x})}{\partial x^m} \simeq \int_\Omega \frac{\partial f(\mathbf{s})}{\partial s^m} W(\mathbf{x}-\mathbf{s})\,\mathrm{d}\mathbf{s} = -\int_\Omega f(\mathbf{s})\frac{\partial W(\mathbf{x}-\mathbf{s})}{\partial s^m}\,\mathrm{d}\mathbf{s} = \int_\Omega f(\mathbf{s})\frac{\partial W(\mathbf{x}-\mathbf{s})}{\partial x^m}\,\mathrm{d}\mathbf{s} \tag{5}$$

Applying a Riemann quadrature to evaluate the integral in (4) gives the SPH approximation for f as

$$f^{\mathrm{a}}(\mathbf{x}) = \sum_{j=1}^{N} \frac{m_j}{\rho_j} f(\mathbf{x}_j)W(\mathbf{x}-\mathbf{x}_j) \tag{6}$$

where the superscript a denotes the approximant, N is the number of used particles with fixed masses m_j and with positions $\mathbf{x}_j$. The variable ρ_j refers to the density of the particle j. Note that the ratio m_j/ρ_j is the volume V_j of particle j, which may vary for compressible media.

Also, using Riemann quadrature to evaluate the integral in (5), the co-ordinate derivatives are computed as

$$\left(\frac{\partial f(\mathbf{x})}{\partial x^m}\right)^{\mathrm{a}} = \sum_{j=1}^{N} V_j f(\mathbf{x}_j)\frac{\partial W(\mathbf{x}-\mathbf{x}_j)}{\partial x^m} \tag{7}$$

The expression of the co-ordinates derivatives $(\partial f/\partial x^m)^{\mathrm{a}}$ can also be obtained by directly differentiating Equation (6), this provides the identity $(\partial f/\partial x^m)^{\mathrm{a}} = \partial f^{\mathrm{a}}/\partial x^m$. This property is not valid if the kernel does not have antisymmetric gradient. In fact, to ensure the zero-order consistency (or the so-called partition of unity) conditions in a discrete form, namely

$$\sum_{j=1}^{N} V_j W(\mathbf{x}-\mathbf{x}_j) = 1$$

and

$$\sum_{j=1}^{N} V_j \nabla W(\mathbf{x}-\mathbf{x}_j)=0$$

a corrected kernel (Shepard function) is often used as [14, 21]

$$W^{\mathrm{c}}(\mathbf{x}-\mathbf{x}_i)=C(\mathbf{x})W(\mathbf{x}-\mathbf{x}_i) \tag{8}$$

with $C^{-1}(\mathbf{x})=\sum_{j=1}^{N} V_j W(\mathbf{x}-\mathbf{x}_j)$. However, this corrected kernel is not in general symmetric (even if the original kernel is symmetric), and its gradient is not antisymmetric. Thus, care must be taken to compute the co-ordinate derivatives. For instance, according to definition (4) and using the above corrected kernel, with W symmetric and with compact support, it follows:

$$\begin{aligned}\frac{\partial f(\mathbf{x})}{\partial x^m} &\simeq \int_{\Omega} \frac{\partial f(\mathbf{s})}{\partial s^m} W^{\mathrm{c}}(\mathbf{x}-\mathbf{s})\,\mathrm{d}\mathbf{s} = -\int_{\Omega} f(\mathbf{s})\,C(\mathbf{x})\frac{\partial W(\mathbf{x}-\mathbf{s})}{\partial s^m}\,\mathrm{d}\mathbf{s}\\ &= \int_{\Omega} f(\mathbf{s})\,C(\mathbf{x})\,\frac{\partial W(\mathbf{x}-\mathbf{s})}{\partial x^m}\,\mathrm{d}\mathbf{s}\end{aligned}$$

Thus, applying Riemann quadrature the approximate derivative is written as

$$\left(\frac{\partial f}{\partial x^m}\right)^{\mathrm{a}}(\mathbf{x})=\sum_{j=1}^{N} V_j\, f(\mathbf{x}_j)\,C(\mathbf{x})\;\left.\frac{\partial W(\mathbf{x}-\mathbf{s})}{\partial s^m}\right|_{s=x_j}$$

It can be seen that $(\partial f/\partial x^m)^{\mathrm{a}} \neq \partial f^{\mathrm{a}}/\partial x^m$.

Remark 1
By applying formula (7), the discrete derivative computed at the particle position $\mathbf{x}_i$ is

$$\nabla f(\mathbf{x}_i)^{\mathrm{a}}=\sum_{j=1}^{N} V_j f(\mathbf{x}_j)\nabla W_{ij}$$

with $\nabla W_{ij}=\nabla W(\mathbf{x}-\mathbf{x}_j)|_{\mathbf{x}=\mathbf{x}_i}$. For example, consider a distribution of particles in one dimension, spaced by $\mathrm{d}x$, and a symmetric kernel with a smoothing length $l=\mathrm{d}x/2$. In this case $V_j=\mathrm{d}x$. The approximate derivative is then given by $\mathrm{d}f(\mathbf{x}_i)^{\mathrm{a}}/\mathrm{d}x=\mathrm{d}x\,(\mathrm{d}W_{i,i+1}/\mathrm{d}x)\,(f_{i+1}-f_{i-1})$. It can be zero for non-trivial solutions such as $f_i=(-1)^i$. These oscillating solutions are spurious modes for the discrete gradient operator. This is an instability issue well known in the context of finite difference and finite elements methods, where the gradient is approximated by centred difference schemes. It is interesting to note that the best accuracy that can be obtained by a two-nodes stencil corresponds to the case where $\mathrm{d}x\,(\mathrm{d}W_{i,i+1}/\mathrm{d}x)=1/2\,\mathrm{d}x$, while the worst case corresponds to $\mathrm{d}W_{i,i+1}/\mathrm{d}x=0$. Clearly, the accuracy is related to the choice of the kernel and its smoothing length. If the latter is too small there may not be enough particles in the support domain, of radius κl, which results in low accuracy. In contrast, if it is too large, local features of the solution may be smoothed out. In our numerical experiments we will choose $\kappa=2$ and a constant smoothing length equal to two times the initial particle spacing.

Let us recall the application of the SPH method for the momentum gas dynamic equations:

$$\frac{\mathrm{D}\mathbf{u}}{\mathrm{D}t} + \frac{\nabla p}{\rho} = 0 \tag{9}$$

where $\mathbf{u}$ is the velocity and p the pressure. For a particle i, the nodal acceleration is classically computed by

$$\frac{\mathrm{D}\mathbf{u}_\mathrm{i}}{\mathrm{D}t} = -\sum_{j=1}^{N} m_j \left(\frac{p_j}{\rho_j^2} + \frac{p_i}{\rho_i^2} \right) \nabla W_{ij} \tag{10}$$

In order to damp the oscillations near shocks and to avoid interpenetration of particles, an artificial viscosity was proposed by Monaghan [19] and is given by

$$\Pi_{ij} = \begin{cases} -\alpha \tilde{c}_{ij} \mu_{ij} + \beta \tilde{c}_{ij} \mu_{ij}^2 & \text{if } (\mathbf{u}_i - \mathbf{u}_j) \cdot (\mathbf{x}_i - \mathbf{x}_j) < 0 \\ 0 & \text{elsewhere} \end{cases} \tag{11}$$

where α and β are constants, $\tilde{c}_{ij}$ is the average of wave speed associated with particles i and j and $\mu_{ij} = l(\mathbf{u}_i - \mathbf{u}_j) \cdot (\mathbf{x}_i - \mathbf{x}_j)/((\mathbf{x}_i - \mathbf{x}_j)^2 + \varepsilon^2)$. The parameters α and β are often taken, respectively, as 0.01 and 0 [12]. Thus, the stabilized discrete momentum equations read

$$\frac{\mathrm{D}\mathbf{u}_i}{\mathrm{D}t} = -\sum_{j=1}^{N} m_j \left(\frac{p_j}{\rho_j^2} + \frac{p_i}{\rho_i^2} + \Pi_{ij} \right) \nabla W_{ij} \tag{12}$$

2.2. *The standard SPH method for SWE*

One can use an analogy between isentropic compressible flows and shallow-water flows, as water depth h plays a similar role to density ρ. The SWE are identical to the two-dimensional gas dynamic equations using this analogy and using as the state law $p = gh^2/2$. From Equation (12) it follows that the SPH discrete form of the momentum equations (2) is obtained as

$$\frac{\mathrm{D}\mathbf{u}_i}{\mathrm{D}t} = -\sum_{j=1}^{N} V_j (g(h_j + h_i) + \Pi_{ij}) \nabla W_{ij} \tag{13}$$

where h_i is the nodal water height of particle i. Note that one of the consistency properties of the kernel, that is $\sum_{j=1}^{N} V_j \nabla W_{ij} = 0$, is used to obtain a symmetric form of Equation (13). The global conservation of the linear momentum can be proved using a consistent kernel with an antisymmetric gradient [19].

Remarks 2

- The continuity equation is implicitly satisfied since a Lagrangian kinematic approach is used, i.e. the particle masses are conserved. Water depth h can then be computed using an SPH approximation

$$h^\mathrm{a}(\mathbf{x}_i) = \sum_{j=1}^{N} h_j V_j W_{ij} = \sum_{j=1}^{N} m_j W_{ij} \tag{14}$$

where $W_{ij} = W(\mathbf{x}_i - \mathbf{x}_j)$. Thus, the smoothed particle height is not equal to the nodal height.

- It can be noted from (12) and (13) that the acceleration of any particle i is obtained directly without any smoothing procedure as done for the pressure gradient. In other words, the left-hand side of (13) is obtained by a 'collocation' procedure while the right-hand side is obtained using a smoothing operation over neighbouring particles. The next section, shows more clearly how both terms can be consistently treated using a variational approach.

3. A STABILIZED VARIATIONAL FORMULATION WITH SPH APPROXIMATION

The SPH approximation (6) can be considered as a finite element interpolation. It can be written as

$$f^{\mathrm{a}}(\mathbf{x}, t) = \sum_{j=1}^{N} N_j(\mathbf{x}) f_j(t) \tag{15}$$

where $N_j(\mathbf{x}) = W(\mathbf{x} - \mathbf{x}_j)V_j$ is the shape function associated with the particle j. However, this is not an interpolant approximation; i.e.

$$N_j(\mathbf{x}_i) \neq \delta_{ij}$$

and consequently $f^{\mathrm{a}}(\mathbf{x}_i) \neq f_i$. This property leads to difficulties in enforcing the Dirichlet boundary conditions with SPH approximation.

3.1. Variational formulation

Let us now consider a hyperbolic system of the form

$$\frac{\mathrm{D}\mathbf{u}}{\mathrm{D}t} + \nabla F = 0 \tag{16}$$

where F is a scalar flux (e.g. for shallow water equations $F = gh$). A weak variational formulation of Equation (16) is given by

$$\int_{\Omega_i} N_i(\mathbf{x} - \mathbf{x}_i) \left(\frac{\mathrm{D}\mathbf{u}}{\mathrm{D}t}\right)^{\mathrm{a}} \mathrm{d}\Omega - \int_{\Omega_i} F \nabla N_i(\mathbf{x} - \mathbf{x}_i)\, \mathrm{d}\Omega + \int_{\Gamma_i} F N_i(\mathbf{x} - \mathbf{x}_i)\mathbf{n}\, \mathrm{d}\Gamma = 0 \tag{17}$$

where Ω_i is the compact support, with boundary Γ_i, associated with particle i, and $\mathbf{n}$ its unit normal vector. When the particle domain is completely embedded in the global computational domain (interior particle), the integral contour term is zero. Many choices are possible to approximate flux F such as a constant equal to $F(\mathbf{x}_i)$ over Ω_i or a smoothed approximation $F^{\mathrm{a}}(\mathbf{x})$. The first choice involves fewer computations and is classically used in standard SPH method. We will denote the approximate flux by $F_h(\mathbf{x})$. In contrast, the SPH time derivative is obtained by 'smoothing particles time derivatives', that is

$$\left(\frac{\mathrm{D}\mathbf{u}}{\mathrm{D}t}\right)^{\mathrm{a}}(\mathbf{x}) = \sum_{j=1}^{N} W(\mathbf{x} - \mathbf{x}_j) V_j \dot{\mathbf{u}}_j \tag{18}$$

with $\dot{\mathbf{u}}_j = \mathrm{D}\mathbf{u}_j/\mathrm{D}t$ the nodal particle acceleration and assuming that the smoothing length is not a function of time. Then the first term of Equation (17) becomes

$$\sum_{j=1}^{N} \left(\int_{\Omega_i} W_i V_i W_j V_j \, \mathrm{d}\Omega \right) \dot{\mathbf{u}}_j = \sum_{j=1}^{N} M_{ij} \dot{\mathbf{u}}_j$$

where M_{ij} are the mass matrix coefficients and $W_i = W(\mathbf{x} - \mathbf{x}_i)$. By applying the classical lumping procedure to the consistent mass matrix (i.e. concentrating all the neighbouring masses to particle i),

$$\sum_{j=1}^{N} M_{ij} = \int_{\Omega_i} W_i V_i \left(\sum_{j=1^n} W_j V_j \right) \mathrm{d}\Omega$$

and since $\sum_{j=1}^{N} W_j V_j = 1$, we obtain

$$\sum_{j=1}^{N} M_{ij} = \int_{\Omega_i} W_i V_i \, \mathrm{d}\Omega = V_i$$

If the consistent mass matrix is replaced by its lumped form, Equation (17) becomes

$$\dot{\mathbf{u}}_i - \int_{\Omega_i} F \, \nabla W(\mathbf{x} - \mathbf{x}_i) \, \mathrm{d}\Omega = 0 \tag{19}$$

Using a Riemann quadrature to compute the integrals, the above equation is transformed into

$$\dot{\mathbf{u}}_i - \sum_{j=1}^{N} V_j F_h(\mathbf{x}_j) \, \nabla W_{ji} = 0$$

In the case of a consistent kernel with an antisymmetric gradient, $\sum_{j=1}^{N} V_j F_h(\mathbf{x}_i) \, \nabla W_{ij} = 0$ and $\nabla W_{ji} = -\nabla W_{ij}$. The final SPH discrete form corresponding to problem (17) is

$$\dot{\mathbf{u}}_i = -\sum_{j=1}^{N} V_j (F_h(\mathbf{x}_i) + F_h(\mathbf{x}_j)) \nabla W_{ij} \tag{20}$$

If we consider the case of a corrected kernel with a compact support as given by (8), then the variational problem (17) is rewritten as

$$\int_{\Omega_i} N_i^{\mathrm{c}}(\mathbf{x} - \mathbf{x}_i) \left(\frac{\mathrm{D}\mathbf{u}}{\mathrm{D}t} \right)^{\mathrm{a}} \mathrm{d}\Omega = \int_{\Omega_i} F \, \nabla N_i^{\mathrm{c}}(\mathbf{x} - \mathbf{x}_i) \, \mathrm{d}\Omega \tag{21}$$

Using the numerical quadrature and considering the fact that $\sum_{j=1}^{N} V_j \nabla W_j^{\mathrm{c}} = 0$, the right-hand side term is developed as

$$\sum_{j=1}^{N} V_j (F_h(\mathbf{x}_j) + F_h(\mathbf{x}_i))(C(\mathbf{x}_j) \nabla W(\mathbf{x} - \mathbf{x}_i)_{\mathbf{x} = \mathbf{x}_j} + W(\mathbf{x}_j - \mathbf{x}_i) \nabla C(\mathbf{x}_j))$$

Since W is symmetric, $\nabla W(\mathbf{x} - \mathbf{x}_i)_{\mathbf{x} = \mathbf{x}_j} = -\nabla W_{ij}$. Applying the lumping procedure for the left-hand side of (21), the variational discrete problem is stated as

$$\dot{\mathbf{u}}_i = -\sum_{j=1}^{N} V_j (F_h(\mathbf{x}_j) + F_h(\mathbf{x}_i)) \, (C(\mathbf{x}_j) \nabla W_{ij} - W_{ij} \, \nabla C(\mathbf{x}_j)) \tag{22}$$

Remark 3

It can be concluded that the standard SPH formulation can only be obtained by using a consistent symmetric kernel having a compact support, by applying a mass lumping and assuming a discrete flux $F_h(\mathbf{x}) = F(\mathbf{x}_i)$. Instead of employing a lumped mass matrix, it is possible to use the consistent one for better time accuracy, but this requires the solution of a linear system for every particle and for every time step. It is important to emphasize that the variational formulations (20) and (22) were derived under the assumption of a kernel with a compact support, so the boundary integral terms were canceled.

3.2. Stablization

Let us now consider the issue of stabilizing the variational SPH formulation (20) or (22). As previously stated, standard SPH approximation for the flux gradient yields an instable centred difference scheme. The resulting spurious spatial oscillations may grow in amplitude especially near discontinuities and thus pollute the whole solution. Some stabilizing mechanism has to be introduced in the discrete formulation. The following analysis will be based on the analogy with the approximate Riemann solvers. Such analysis will lead to the development of an artificial viscosity which performs better than that given by Equation (11). We will consider the following Gaussian and spline kernels, which are corrected later to ensure numerical consistency, defined, respectively, by

$$W(\mathbf{x} - \mathbf{x}_i) = \frac{1}{(l\sqrt{\pi})^d} \exp(-\zeta^2)$$

and

$$W(\mathbf{x} - \mathbf{x}_i) = \begin{cases} 4 - 6\zeta^2 + 3\zeta^3 & \text{if } (0 \leqslant \zeta < 1) \\ (2 - \zeta)^3 & \text{if } (1 \leqslant \zeta < 2) \\ 0 & \text{if } (\zeta \geqslant 2) \end{cases}$$

where $\zeta = \|\mathbf{x} - \mathbf{x}_i\|/l$ and d is the space dimension. The following relation holds:

$$\mathbf{n}_{ij} = \frac{\nabla W_{ij}}{|\nabla W_{ij}|} = \frac{\mathbf{r}_{ij}}{|\mathbf{r}_{ij}|}$$

where $\mathbf{r}_{ij} = \mathbf{x}_i - \mathbf{x}_j$ is the distance vector between particles i and j.

Equation (20) suggests that the flux is computed at the mid-distance between particles i and j, as can be seen more clearly in the following relation:

$$\dot{\mathbf{u}}_i = -\sum_j 2V_j \frac{(F_h(\mathbf{x}_j) + F_h(\mathbf{x}_i))}{2} |\nabla W_{ij}| \, \mathbf{n}_{ij}$$

In order to introduce a stabilizing mechanism in the flux computation, a simple Lax–Friedrichs scheme [22] is used. Thus, the centred flux $(F_h(\mathbf{x}_j) + F_h(\mathbf{x}_i))/2$ is replaced by

$$\tfrac{1}{2}((F_h(\mathbf{x}_j) + F_h(\mathbf{x}_i)) - \lambda(\mathbf{u}_j - \mathbf{u}_i) \cdot \mathbf{n}_{ij})$$

with λ a characteristic wave speed. Then, the stabilized SPH formulation reads

$$\dot{\mathbf{u}}_i = -\sum_j V_j \nabla W_{ij} ((F_h(\mathbf{x}_j) + F_h(\mathbf{x}_i)) - \lambda(\mathbf{u}_j - \mathbf{u}_i) \cdot \mathbf{n}_{ij})$$

Consequently, the stabilizing term (in the direction $\mathbf{n}_{ij}$) corresponds to

$$\Pi_{ij} = -\lambda(\mathbf{u}_j - \mathbf{u}_i) \cdot \mathbf{n}_{ij}$$

The unit vector $\mathbf{n}_{ij}$ can be written using the distance vector $\mathbf{r}_{ij}$ which leads to the expression

$$\Pi_{ij} = -\frac{\lambda(\mathbf{u}_j - \mathbf{u}_i) \cdot \mathbf{r}_{ij}}{\sqrt{\mathbf{r}_{ij}^2 + \varepsilon^2}} \tag{23}$$

where ε is a small constant used to avoid a division by zero.

The above stabilized SPH formulation can be applied in a straightforward way to the shallow water momentum equations with the flux function defined by $F = gh$. If its approximation is taken as $F_h(\mathbf{x}_i) = gh_i$ then the standard SPH method given by (13) is found. But, it is possible to choose $F_h(\mathbf{x}_i) = gh_i^{\mathrm{a}}$ to find the following formulation:

$$\dot{\mathbf{u}} = -\sum_{j=1}^{N} V_j \nabla W_{ij} (g(h_i^{\mathrm{a}} + h_j^{\mathrm{a}}) + \Pi_{ij}) \tag{24}$$

which is expected to be more stable. If a corrected kernel is used, then the above equation becomes

$$\dot{\mathbf{u}}_i = -\sum_{j=1}^{N} V_j \, (g(h_i^{\mathrm{a}} + h_j^{\mathrm{a}}) + \Pi_{ij})(\nabla W_{ij} - W_{ij} \nabla C(\mathbf{x}_j)) \tag{25}$$

The continuity equation (14) provides the time evolution for the smoothed water height and not for nodal value h_i. Thus the volumes V_j are computed by $V_j = m_j / h_j^{\mathrm{a}}$. The stabilizing term is given by

$$\Pi_{ij} = -\frac{\lambda_{ij} \mathbf{u}_{ij} \cdot \mathbf{r}_{ij}}{\sqrt{\mathbf{r}_{ij}^2 + \varepsilon^2}} \tag{26}$$

where $\mathbf{u}_{ij} = \mathbf{u}_i - \mathbf{u}_j$ is the relative velocity, $\lambda_{ij} = (c_i + c_j)/2$ and $c_i = \sqrt{g h_i^{\mathrm{a}}}$ is the pressure wave speed. Contrary to Monaghan's [19] artificial viscosity, expression (26) is not dependent on the smoothing length l or on the free parameter α. Also, it does not vanish for particles moving in the same or opposite directions, so it prevents the stencil spurious oscillations from being generated.

4. BOUNDARY CONDITIONS AND TEMPORAL DISCRETIZATION

We will now focus on the treatment of the boundary conditions, especially on solid walls, using the SPH method. This treatment is not an easy task, as seen above due to the non-interpolant and Lagrangian character of the SPH formulation and the condition that the kernel has compact support. Indeed, it is difficult to ensure a compact support for the particles in the vicinity of the wall, since there is no control of their motion. We treated simple geometrical configurations. We mainly used two methods: the ghost particles method and the symmetrization method. We will briefly introduce these techniques in the following sections. We have also used the force method of Monaghan [19] but it gave poor results in our numerical experiments.

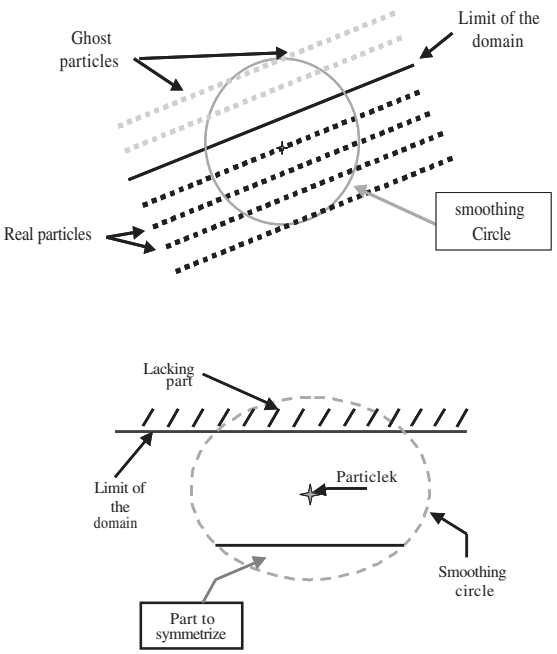

Figure 1. Ghost particles method (top), symmetrization method (bottom).

4.1. The Ghost particles method

This method consists of adding new particles around the boundary on the missing part of the smoothing support (Figure 1). In the case of a perfect slipping boundary condition, the values of the tangential velocity attributed to these particles are the same as the real ones and the opposite ones for the normal component. Thus we obtain a purely tangential velocity on the limit of the domain. In the case of a perfect friction condition, the opposite of the tangential component is attributed to the ghost particles.

4.2. The symmetrization method

A second method used in our work is symmetrization. This can be described briefly as follows: for any particle in the vicinity of the boundary, i.e. with an incomplete smoothing support, a detection of both the missing part and its symmetric is done (Figure 1). Thus, the computation of the velocity uses twice the real part which has been detected (in case of a perfect slipping condition). Consequently, the particle in the vicinity of the boundary will have a full contribution from its neighbours as if it was in the middle of the domain (the missing part is compensated for by its corresponding symmetric part). It should be noted that this second method has a lower cost than the ghost particles method as there are no new added particles. However, it is used only with simple geometries and might be hard to apply in case of complex boundaries.

4.3. Time discretization

An explicit Newmark scheme is used for time discretization. The velocity and the co-ordinates for a particle i are obtained as

$$\mathbf{u}_i^{n+1} = \mathbf{u}_i^n + \Delta t((1-\gamma)\dot{\mathbf{u}}_i^n + \gamma\dot{\mathbf{u}}_i^{n+1}) \tag{27}$$

$$\mathbf{x}_i^{n+1} = \mathbf{x}_i^n + \Delta t\,\mathbf{u}_i^n + \Delta t^2((\tfrac{1}{2}-\beta)\dot{\mathbf{u}}_i^n + \beta\dot{\mathbf{u}}_i^{n+1}) \tag{28}$$

where Δt is the time step, $\mathbf{u}$ is the velocity, $\dot{\mathbf{u}}$ is the acceleration and the notation $\mathbf{u}^n$ means $\mathbf{u}(t^n)$. By choosing the parameters β and γ equal, respectively, to $\frac{1}{4}$ and $\frac{1}{2}$ the scheme corresponds to the trapezoidal rule and is second-order accurate.

Remark 4 (*Neighbours search algorithm*)
In mesh-based methods, the connectivity between the nodes is known once the grid is given. In Lagrangian meshless methods such as the SPH, the connectivity between the particles varies in time. Thus, at each time step, the nearest neighbouring particles for every specified particle have to be found. This search process takes most of the computing time so it has to be done efficiently. For two-dimensional problems we used the octree algorithm [7]. A structured grid is overlaid on the problem domain (Figure 2). The mesh spacing selected equals the radius of the support domain, i.e. κl. Thus, for a given particle the cell where it belongs is first determined. The nearest neighbours are then located in that cell and in its eight adjacent cells. Note that the temporary grid is only used for the neighbours search and not for any numerical integration purpose.

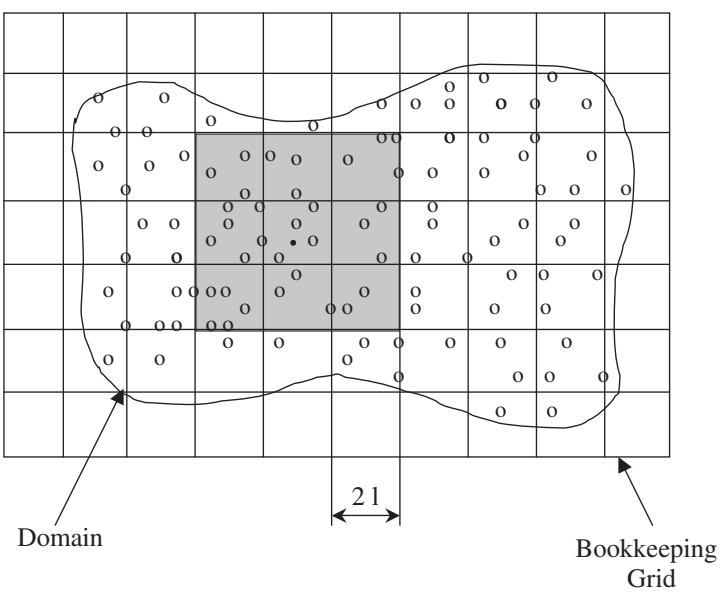

Figure 2. The octree algorithm for neighbours searching.

The overall algorithm applied to SWE can be summarized in the following computational steps:

- Initial conditions: given $h_j^0, \mathbf{u}_j^0, V_j^0$
- Loop over time steps: Do $n = 1, \ldots$
- Loop over particles: Do $i = 1, N$;
  - update the list of neighbours,
  - compute acceleration: $\dot{\mathbf{u}}^{n+1} = -\sum_{j=1}^{N} V_j^n \nabla W_{ij}(g(h_i^a + h_j^a) + \Pi_{ij})^n$
  - update velocity: $\mathbf{u}_i^{n+1} = \mathbf{u}_i^n + \Delta t/2(\dot{\mathbf{u}}_i^n + \dot{\mathbf{u}}_i^{n+1}))$
  - update co-ordinates: $\mathbf{x}_i^{n+1} = \mathbf{x}_i^n + \Delta t \mathbf{u}_i^n + \Delta t^2/4(\dot{\mathbf{u}}_i^n + \dot{\mathbf{u}}_i^{n+1})$
  - update smoothed water heights: $h_i^{a(n+1)} = \sum_{j=1}^{N} m_j W_{ij}^{(n+1)}$.
- Enddo, Enddo.

5. NUMERICAL RESULTS

In the following section, some numerical experiments are performed to assess the techniques discussed previously. The dam break problem in one- and two-dimension is taken as the primary benchmark test. The initial conditions are shown in Figure 3. The depth of water is 10 m upstream and 1 m downstream. All results are compared with the exact solution [23].

5.1. The dam break problem in one dimension

The first set of numerical experiments is aimed at comparing the results obtained with different variants of the variational formulations and the artificial viscosities. The effect of the smoothing length is also assessed. Formulation (25) is considered with the Gaussian kernel and a smoothing length equals twice the initial spacing of particles dx. The time step used is $\Delta t = 0.02$ s. All the following figures show the water height results at time $t = 30$ s. Figure 4 shows a comparison between the results obtained using the new artificial viscosity (26) and the standard one (11). In this test case, 1000 particles are used along with the Gaussian kernel

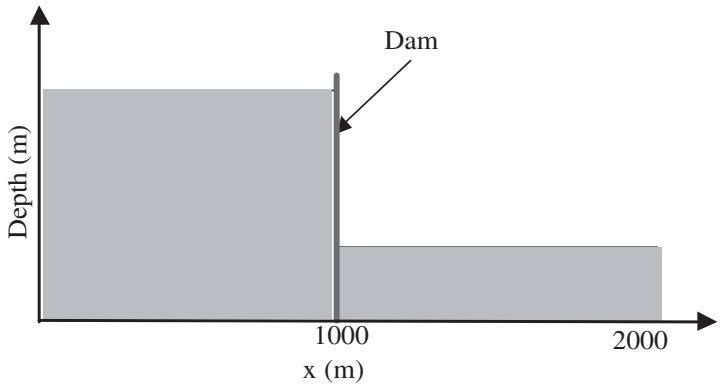

Figure 3. Initial conditions for the dam break problem.

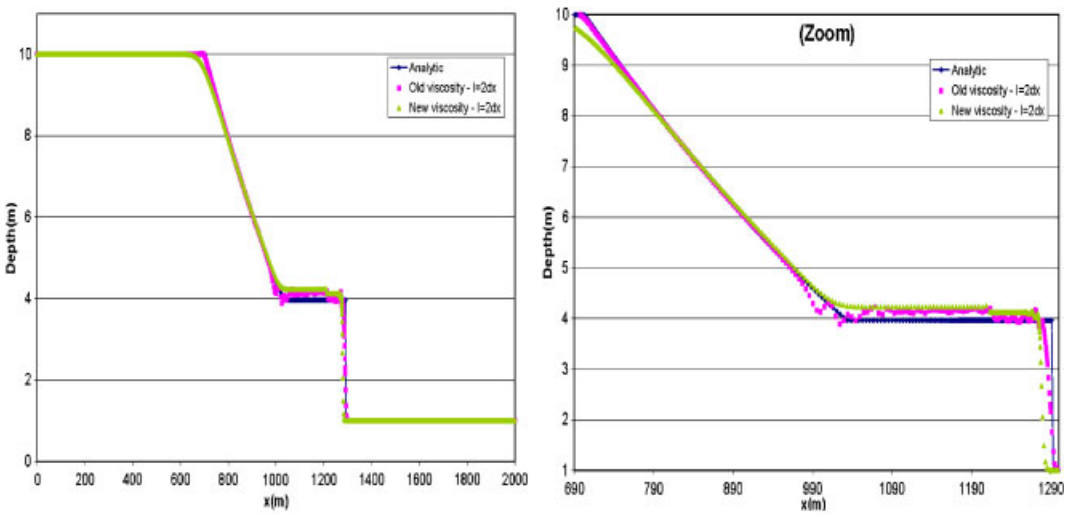

Figure 4. Comparison between the new and the old viscosities, right figure is a zoom of the left one.

and formulation (20). The best result for the Monaghan's viscosity is obtained for $\alpha = 2.0$ and $\beta = 0.0$. Most of the spurious oscillations are eliminated with the new viscosity, but there are still a few wiggles near the shock. The plateau is well defined, but its value is high, with a little kick located at the original position of the discontinuity. There is a smearing of the water height in the rarefaction wave caused more likely by the diffusion effect of the artificial viscosity. This could be reduced if a limiter were used as usually adopted in high-order FV-MUSCL methods.

Formulation (25) is then considered, where the kernel gradient is fully corrected. The results are shown in (Figure 5). The plateau is now closer to its exact value but there are still a few oscillations in the shock and the diffusion effect is clear. We found experimentally that the best results were obtained if a partial correction of the kernel gradient was used, i.e. when the gradient of $C(x)$ in formulation (25) is neglected (Figure 5). This can be explained by the fact that the numerical integration (collocation method) introduces larger errors to integrate the gradient. Indeed, the corrected kernel is a rational function with a gradient having a strong non-polynomial character. The shock is sharper and the plateau is closer to the exact solution.

The next tests were performed with $l = 3\,\mathrm{d}x$ (Figure 6). The solutions are clearly more smeared with best results obtained with the new viscosity and a partially corrected kernel gradient. A convergence test is finally considered using $l = 2\,\mathrm{d}x$, the new viscosity and a partially corrected kernel gradient. Clearly the solution is enhanced by increasing the number of particles (Figures 7 and 8). The maximum and euclidian error norms are shown in Figure 9, the rate of convergence seems slow.

5.2. The dam break problems in 2D

Two-dimensional test cases were performed in order to show again the effects of the new stabilization viscosity and the treatment of solid boundary conditions. Two geometrical

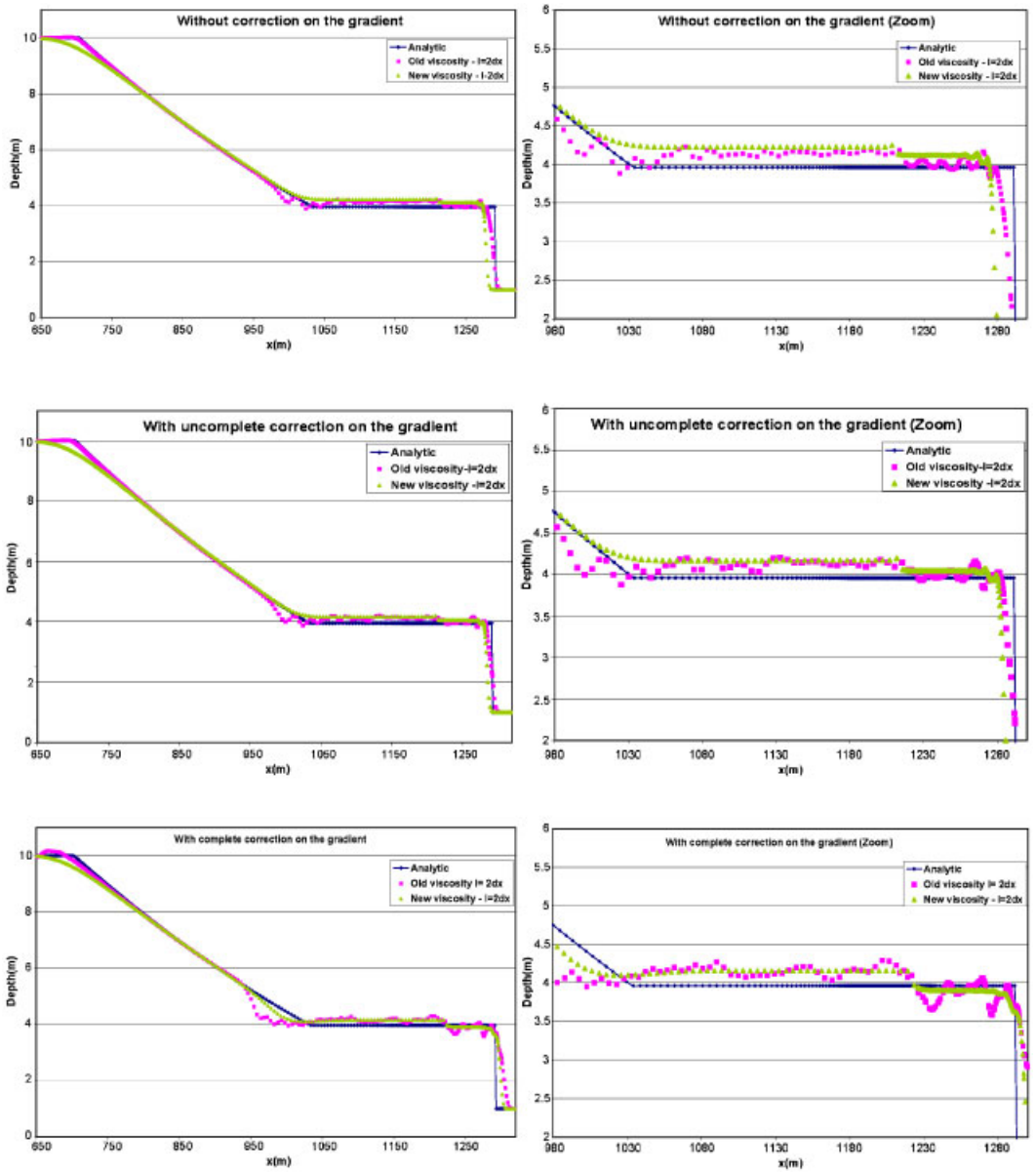

Figure 5. Effect of the new viscosity in one-dimensional case—smoothing length $l = 2\Delta x$. Up: no correction on the gradient, middle: incomplete correction, down: complete correction. Right figures are the zooms of the left ones.

configurations will be presented. We will start with the standard dam in an open rectangular channel. When the geometry is relatively simple, as in the rectangular channel, we used the ghost particles method. It consists of adding some virtual particles so that the smooth-

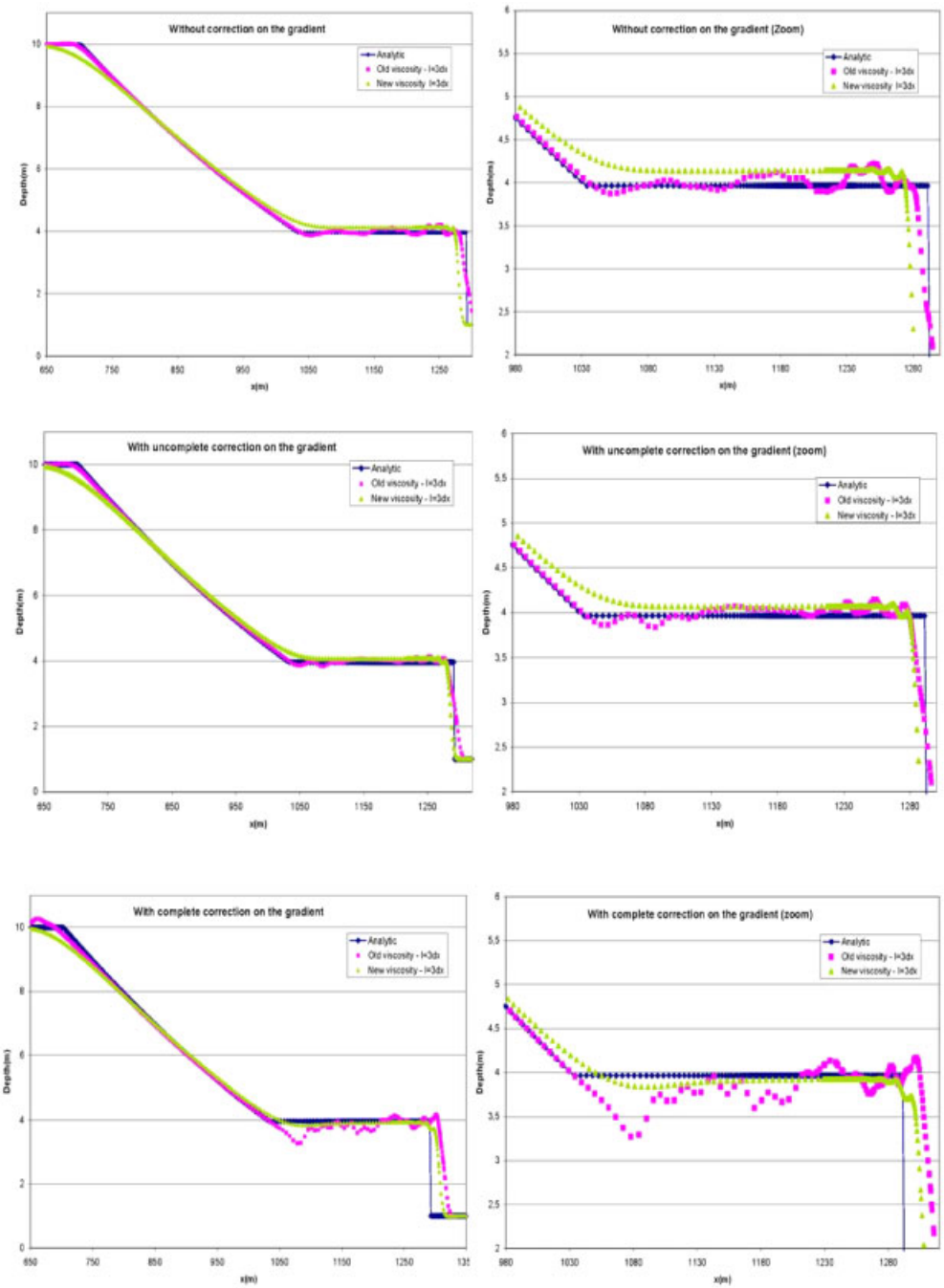

Figure 6. Effect of the new viscosity in one-dimensional case—smoothing length $l = 3\Delta x$. Up: no correction on the gradient, middle: incomplete correction, down: complete correction. Right figures are the zooms of the left ones.

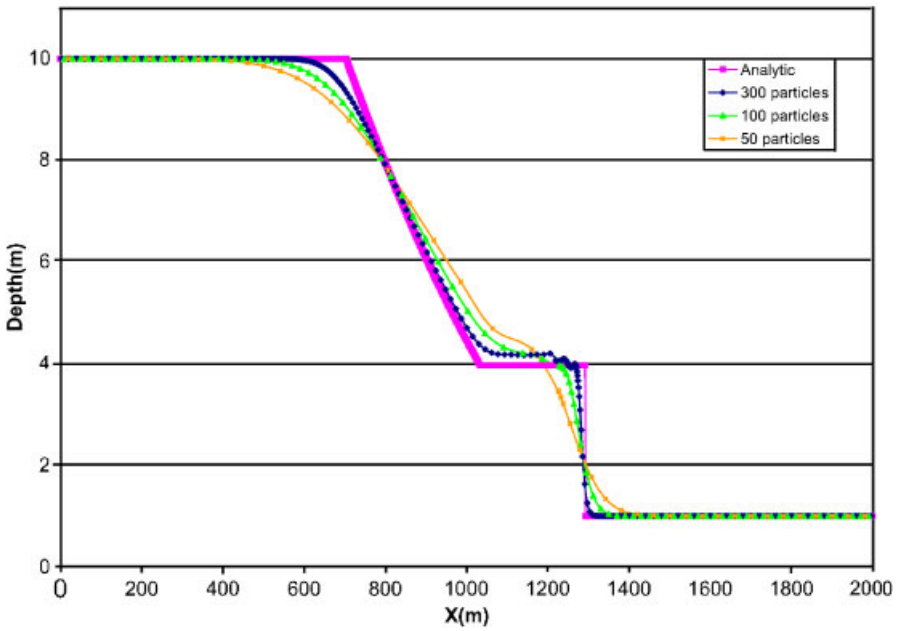

Figure 7. Effect of the number of particles—number of particles between 50 and 300.

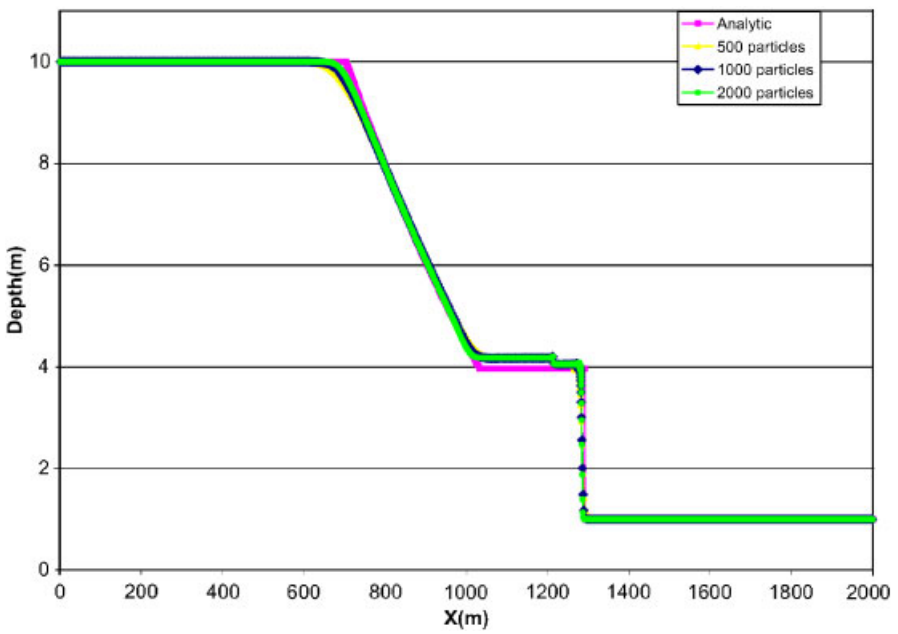

Figure 8. Effect of the number of particles—number of particles between 500 and 2000.

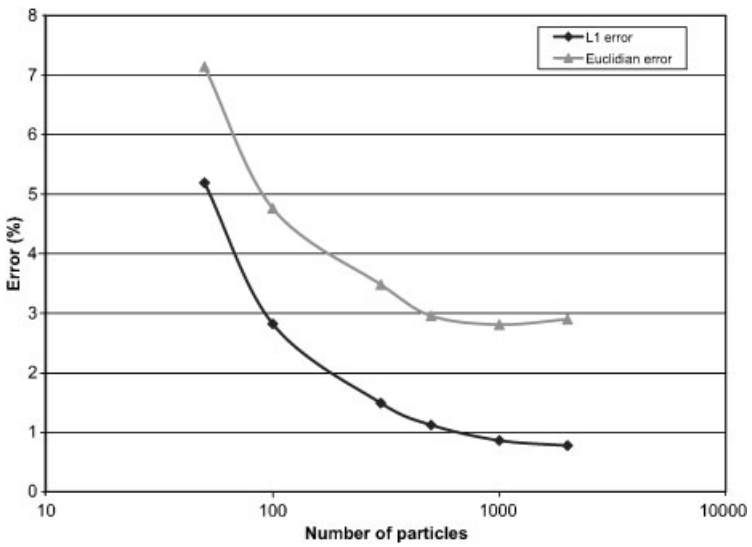

Figure 9. L1 and Euclidian errors: effect of the number of particles.

ing circle is completely full. We used also the symmetrization method which consists on symmetrizing the lacking part of the smoothing circle to get the condition of perfect slipping. Both methods gave almost the same results. The initial conditions were exactly the same as those used in the one-dimensional case. The width of the channel was taken 75 m. We used 10 080 equally spaced particles to fulfil these simulations. The simulation time is 30 s and we used a constant time step of 0.02 s. An increase of the time step until 0.1 s (which corresponds to a maximum CFL condition of almost 0.4) did not affect the accuracy of the solution. The smoothing length was taken as $l = 2\Delta x$ where Δx is the initial distance between two successive particles. As it can be seen in Figure 10, the new viscosity gives better stabilization while there are fewer oscillations, especially in the shock wave and at the location of the contact discontinuity. The shock position remains slightly high even with a large number of particles. This discrepancy can be explained by the combined effect of the diffusive effect of the new viscosity added to the low-order interpolation used. It is necessary here to indicate that for more complicated geometries, the results are not encouraging, particularly, the resolution of the shock is very sensitive to the treatment of the solid boundary conditions.

5.3. Cylindrical dam break problem

The geometrical setting and the initial conditions for the second test case, referred to as the cylindrical dam break problem, are described in Figure 11. We used 40 000 particles corresponding to a structured mesh of (200×200) squares to achieve this simulation. The water depth inside the dam is 2.5 m and 0.5 m outside. The radius of the initial dam is 0.5 m. The domain is a $40 \times 40\,\mathrm{m}^2$. The smoothing length is also $2\Delta x$ and the simulation time is 3.5 s. We used the symmetrization method so that we simulated an infinite domain. In this case we see even more clearly the effect of the new stabilizing viscosity. Figure 12 shows that

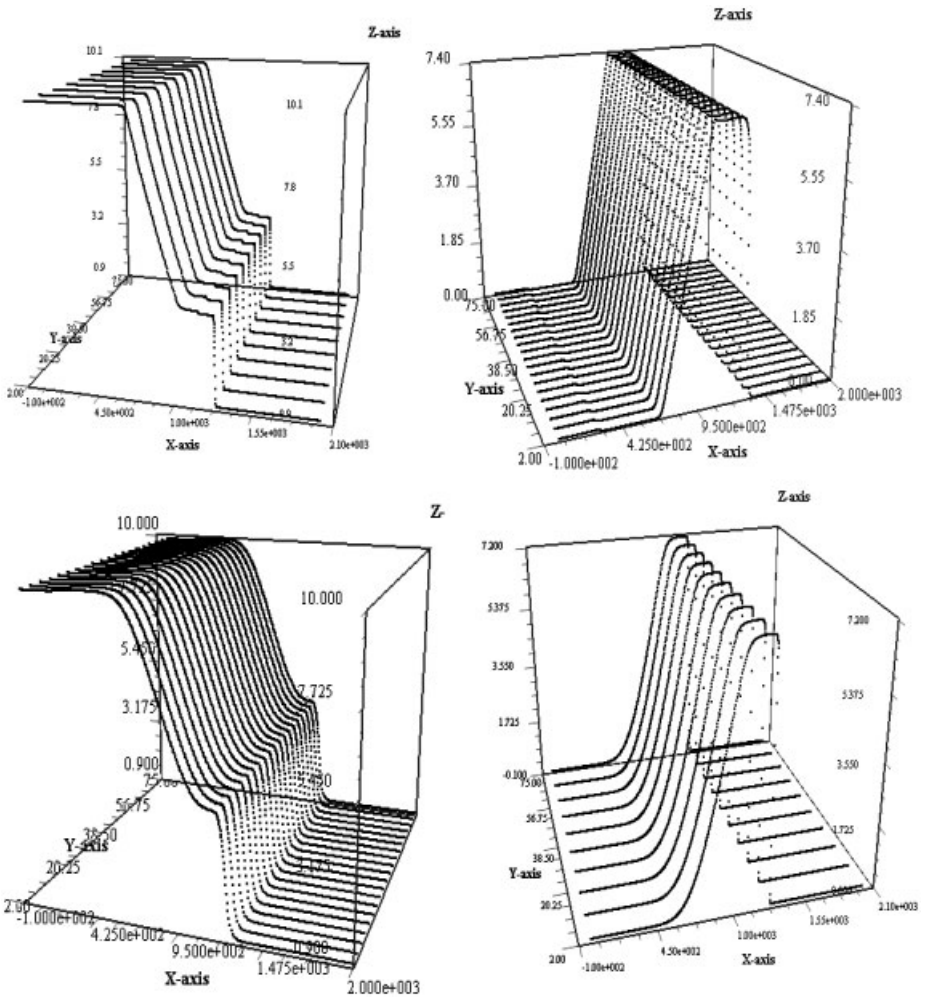

Figure 10. Dam break problem in two-dimensions, effect of the new viscosity: (Up) Water depth (left) and velocity (right) with old viscosity. (Down) Water depth (left) and velocity (right) with new viscosity.

the water elevation has no more oscillations near the shock and rarefaction waves. Compared to the high-order finite volumes results of Toro [22] the SPH results are quite acceptable. For the first two plots, the new SPH scheme appears to deviate from the FVM. This is caused by the diffusive effect of the new viscosity. More precisely, the Lax–Friedrich scheme used does not include any MUSCL-type reconstruction to reduce the dissipation commonly associated with first-order Godunov-type schemes.

It should be noted that the SPH method is generally much slower compared to FVM. The CPU time can exceed 50 times that of the FVM. For instance, for 40 000 particles and for $t = 3.5$ s the CPU time is about 24 min, while for the FVM it takes less then

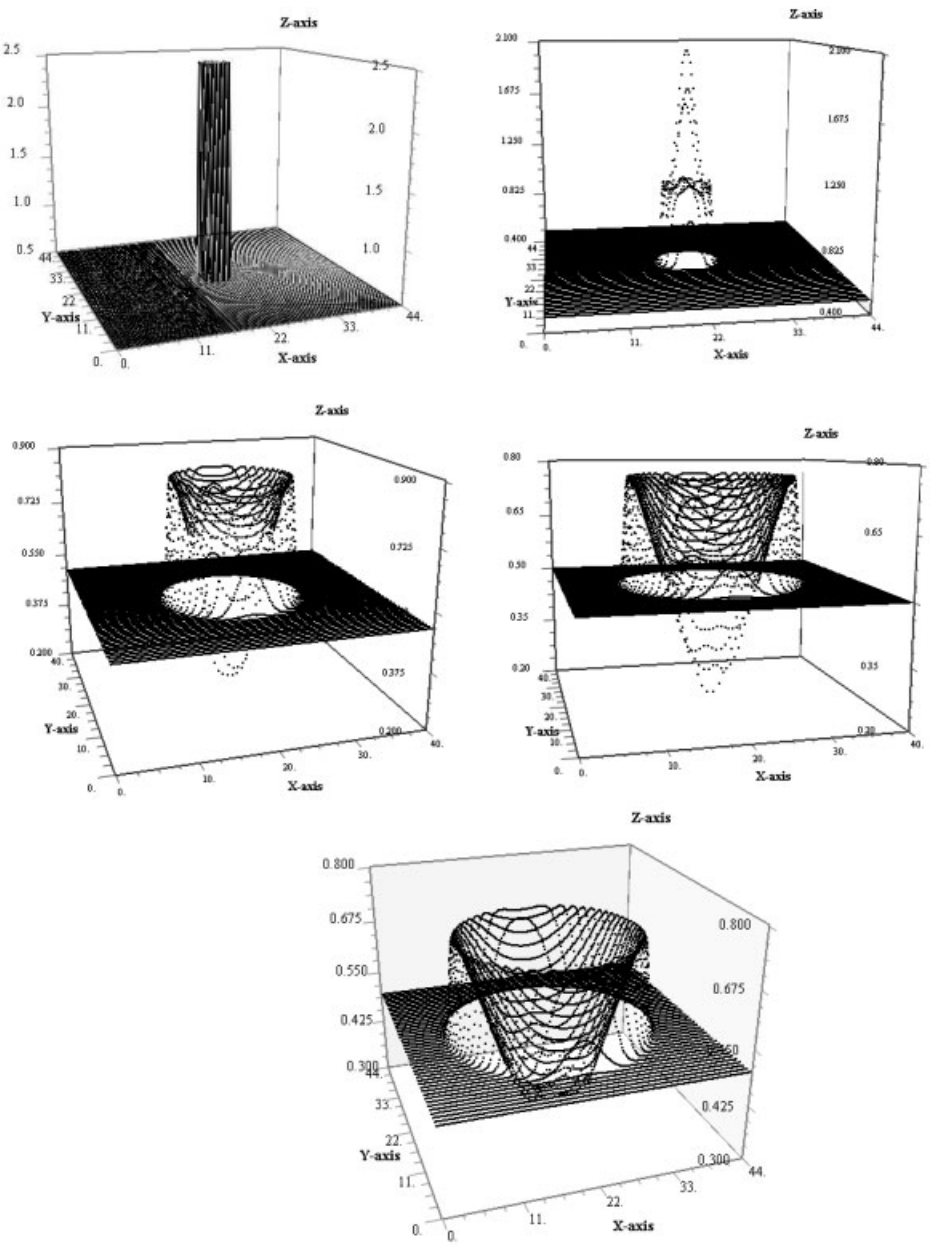

Figure 11. Initial conditions and evolution of the circular dam in the time $t = 0, 0.4, 1.5, 2.5, 3.5$ s.

4 min to achieve the simulation with the same number of cells on a 550 MHz computer. We were able to reduce this factor to almost 6 using the octree algorithm for neighbour sorting [7].

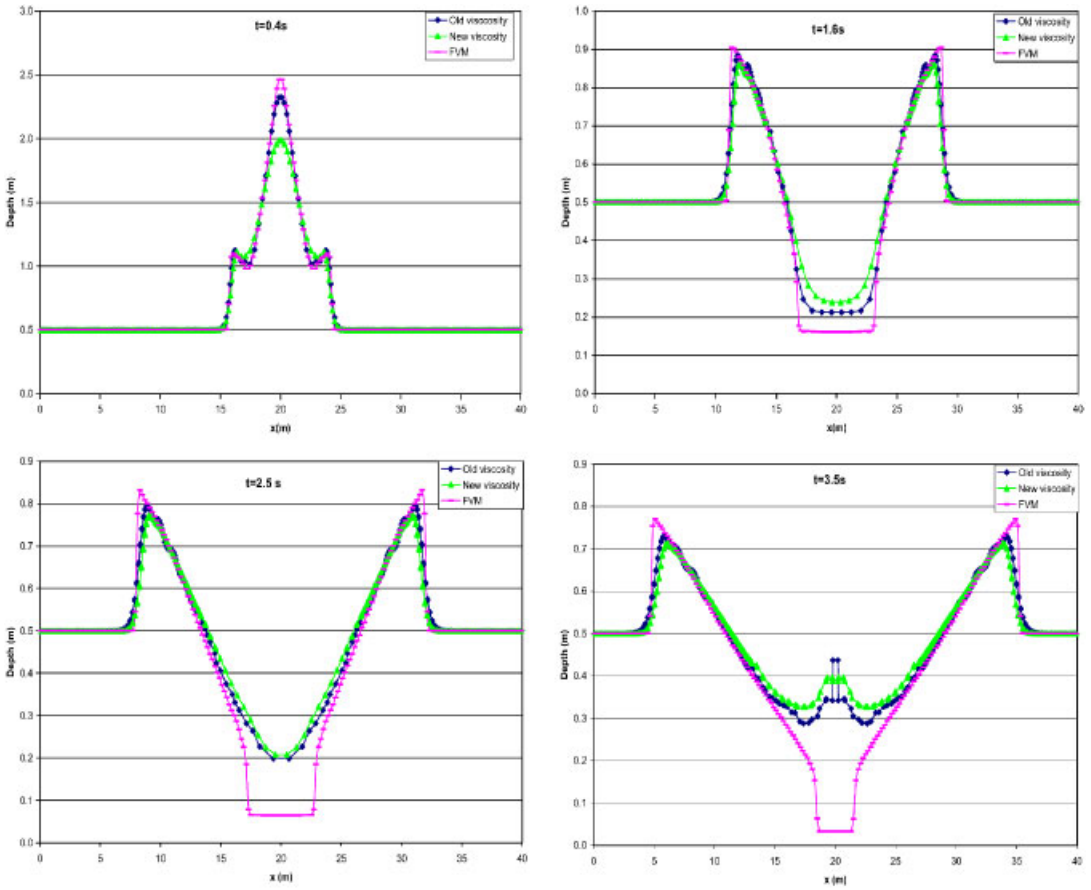

Figure 12. Cylindrical dam. Effect of the new viscosity. Comparison with FVM.

6. CONCLUSION

In this study, we focused on the application of the SPH methodology to the shallow water equations. Standard SPH method has the advantage of being relatively simple to formulate and to implement. We also discussed on variational formulations using SPH interpolations. The partially corrected formulation seems to give better results in conjunction with the collocation numerical integration. A new artificial viscosity is properly derived by using an analogy with an approximate Riemann solver. Several numerical tests have been performed. It is shown that the new stabilization gives better results than the standard artificial viscosity suggested by Monaghan. For bounded domains, serious difficulties are encountered to enforce Dirichlet boundary conditions. Symmetrization and ghost particle techniques have been implemented but do not give good results for irregular boundaries and in presence of shocks. Further studies are required to make the SPH method more competitive with standard approaches.

REFERENCES

1. Lucy LB. A numerical approach to testing of fusion process. *The Astronomical Journal* 1977; **82**:1013–1024.
2. Gingold RA, Monaghan JJ. Smoothed particle hydrodynamics: theory and application to non-spherical stars. *Monthly Notices of the Royal Astronomical Society* 1977; **181**:375–389.
3. Cloutman LD. Basics of smoothed particle hydrodynamics. *Lawrence Livermore National Laboratory Report UCRL-ID*-103698, 1990.
4. Johnson GR. Linking of Lagrangian particle methods to standard finite element methods for high velocity impact computations. *Nuclear Engineering and Design* 1994; **150**:256–274.
5. Johnson GR, Beissel SR. Normalised smoothing functions for SPH impact computations. *International Journal for Numerical Methods in Engineering* 1996; **39**:2725.
6. Letellier A, Bung H, Galon P, Berhillier M. Bird impact on fan blade analysis using SPH coupled with finite elements. *Structure Under Extreme Loading Conditions*, PVP 351. ASME: New York, 1997.
7. Libersky LD, Petshek AG. *Smooth Particle Hydrodynamics with Strength of Materials*. Lecture Notes in Physics, vol. 395. Springer: Berlin, 1990; 248–357.
8. Liu GR, Liu MB. *Smooth Particle Hydrodynamics*, *A Meshfree Particle Method*. World Scientific, 2003.
9. Fries TP, Matthies HG. Classification and overview of meshfree methods. *Technical Report*, Scientific Computing, Technical University, Germany, 2003.
10. Inutsuka SI. Reformulation of smoothed particle hydrodynamics with Riemann solver. *Journal of Computational Physics* 2002; **179**:238–267.
11. Cha SH, Whitworth AP. Implementations and tests of Gudunov-type particle hydrodynamics. *Monthly Notices of the Royal Astronomical Society* 2003; **340**:73–90.
12. Monaghan JJ. Simulating free surface flows with SPH. *Journal of Computational Physics* 1994; **110**(2): 399–406.
13. Frank J, Reich S. Conservation properties of smoothed particle hydrodynamics applied to shallow water equations. *BIT Numerical Mathematics* 2003; **43**(1):41–55.
14. Bonet J, Kulasegaram S, Rodriguez-Paz MX, Profit M. Variational formulation for the smooth particle hydrodynamics (SPH) simulation of fluid and solid problems. *Computer Methods in Applied Mechanics and Engineering* 2004; **193**(12):1245–1257.
15. Wang Z, Shen HT. Lagrangian simulation of one dimensional dam-break flow. *Journal of Hydraulic Engineering* 1999; **125**(11):1216–1220.
16. Monaghan JJ. SPH and Riemann solvers. *Journal of Computational Physics* 1997; **136**:298–307.
17. Stellingwerf RA. *Smooth Particle Hydrodynamics*. Lecture Notes in Physics, vol. 395. Springer: Berlin, 1990; 239–247.
18. LeVeque RJ. Balancing source terms and flux gradients in high-resolution Godunov methods: the quasisteady wave-propagation algorithm. *Journal of Computational Physics* 1998; **146**:346–365.
19. Monaghan JJ. Introduction to SPH. *Computer Physics Communication* 1988; **48**:89–96.
20. Vila JP. On particle weighted methods and smooth particle hydrodynamics. *Mathematical Models and Methods in Applied Sciences* 1999; **9**(2):191–209.
21. Ata R. Les écoulements á surface libre avec la méthode SPH. *Master Thesis* (in French), *École de technologie supérieure*, Université du Québec, 2002.
22. Toro EF. *Shock Capturing Methods for Free Surface Shallow Water Flows*. Wiley: New York, 2001.
23. Stoker JJ. *Water Waves*. Interscience, Wiley: New York, 1957.
24. Ben Moussa B. Analyse numérique de méthodes particulaires regularisées de type SPH pour les lois de conservation. *Thesis*, INSA, Toulouse, France, 1998.
25. Parshikov AN, Medin SA, Loukashenko II, Milekhin VA. Improvements in SPH method by means of interparticle contact algorithm and analysis of perforation tests at moderate projectile velocities. *International Journal of Impact Engineering* 2000; **24**:779–796.
26. Soulaimani A, Idrissi M. Identification of friction coefficient in shallow-water flows using optimal control theory. *International Journal of Computational Fluid Dynamics* 1990; **112**:29–40.
27. Soulaimani A. Nouveaux aspects de l'application de la méthode des élṁents finis en hydrodynamique. *Thése de doctorat*, Publication de l'université Laval, Québec, 1983.

